Received: 6 April 2022 | Revised: 13 February 2023 | Accepted: 23 February 2023

DOI: 10.1002/jbm.a.37526

RESEARCH ARTICLE

In-vivo evaluations of bone regenerative potential of two novel bioactive glasses

A. Anesi[1] | M. Ferretti[2] | R. Salvatori[1] | D. Bellucci[3] | F. Cavani[2] | M. Di Bartolomeo[4] | C. Palumbo[2] | V. Cannillo[3]

[1]Laboratorio Biomateriali, Dipartimento di Scienze Mediche e Chirurgiche Materno-Infantili e dell'Adulto, Università degli Studi di Modena e Reggio Emilia, Modena, Italy

[2]Dipartimento di Scienze Biomediche, Metaboliche e Neuroscienze – Sezione di Morfologia umana (c/o Policlinico), Università degli Studi di Modena e Reggio Emilia, Modena, Italy

[3]Dipartimento di Ingegneria "Enzo Ferrari", Università degli Studi di Modena e Reggio Emilia, Modena, Italy

[4]Chirurgia Maxillo Facciale e Odontostomatologia, Dipartimento di Scienze Chirurgiche Odontostomatologiche e Materno-Infantili, Università degli Studi di Verona, Verona, Italy

Correspondence
D. Bellucci, Dipartimento di Ingegneria "Enzo Ferrari", Università degli Studi di Modena e Reggio Emilia, Via P. Vivarelli 10, 41125 Modena, Italy.
Email: devis.bellucci@unimore.it

F. Cavani, Dipartimento di Scienze Biomediche, Metaboliche e Neuroscienze – Sezione di Morfologia umana (c/o Policlinico), Università degli Studi di Modena e Reggio Emilia, Via Campi 287, 41125 Modena, Italy.
Email: francesco.cavani@unimore.it

Abstract

Due to the aging of population, materials able to repair damaged tissues are needed. Among others, bioactive glasses (BGs) have attracted a lot of interest due to their outstanding properties both for hard and soft tissues. Here, for the first time, two new BGs, which gave very promising results in preliminary in vitro-tests, were implanted in animals in order to evaluate their regenerative potential. The new BGs, named BGMS10 and Bio_MS and containing specific therapeutic ions, were produced in granules and implanted in rabbits' femurs for up to 60 days, to test their biocompatibility and osteoconduction. Additionally, granules of 45S5 Bioglass® were employed and used as a standard reference for comparison. The results showed that, after 30 days, the two novel BGs and 45S5 displayed a similar behavior, in terms of bone amount, thickness of new bone trabeculae and affinity index. On the contrary, after 60 days, 45S5 granules were mainly surrounded by wide and scattered bone trabeculae, separated by large amounts of soft tissue, while in BGMS10 and Bio_MS the trabeculae were thin and uniformly distributed around the BG granules. This latter scenario could be considered as more advantageous, since the features of the two novel BG granules allowed for the neo-formation of a uniformly distributed bony trabeculae, predictive of more favorable mechanical behavior, compared to the less uniform coarse trabeculae, separated by large areas of soft tissue in 45S5 granules. Thus, BGMS10 and Bio_MS could be considered suitable products for tissue regeneration in the orthopedic and dental fields.

KEYWORDS
bioactive glasses (BGs), biocompatibility, bone regeneration, in vivo tests, osteoconductivity, rabbits

1 | INTRODUCTION

Musculo-skeletal problems affect a significant amount of the aging population; it is estimated that hundreds of millions of people all over the world are affected by such pathologies. In this scenario, there is

A. Anesi, M. Ferretti, C. Palumbo, and V. Cannillo contributed equally to this work.

TABLE 1 Composition (mol%) of BGMS10 and Bio_MS.

Glass	Na_2O	K_2O	CaO	MgO	SrO	P_2O_5	SiO_2
BGMS10[24,25]	2.3	2.3	25.6	10.0	10.0	2.6	47.2
Bio_MS[26]	5.0	-	31.3	5.0	10.0	2.6	46.1

an increasing need for materials able to replace missing or damaged tissues and capable of contributing to healing. Due to the inherent limitations of autologous or heterologous implants (such as pain in the donor site and possible transmission of pathogens), synthetic materials actually play a major role in tissue regeneration.[1–3] Among others, bioceramics and in particular bioactive glasses (BGs) have been extensively used in recent years, due to their well-known biocompatibility and regenerative potential. BGs, since their discovery by Hench in 1969,[4] have had a disruptive effect in the field of tissue engineering, displaying outstanding properties both for hard and soft tissues.[5,6] Additionally, BGs can elicit an antibacterial effect, which has been proven to be very beneficial for bone regeneration and healing.[7–9]

The main disadvantage associated with these materials, and in particular with the original composition 45S5 Bioglass® (from here on referred as 45S5), is their fast tendency to crystallize at relatively low temperatures (at ≈600°C), when subjected to heat treatments required to obtain sintered products, for example, coatings, scaffolds, and so forth.[10–12] As a matter of fact, such sintered parts are characterized by a reduced bioactivity. Moreover, crystallization can be dangerous, since it may lead to the instability of the implant, because the residual glassy phase is preferentially degraded by the surrounding biological environment. Additionally, it should be noted that the ionic release—which is crucial for the osteogenesis and angiogenesis—might be very slow in partially crystallized samples; it is important to stress that the regenerative potential of BGs is markedly influenced by their ionic release.[13,14]

Recently, a lot of effort has been put to design alternative formulations, both to lower the tendency to crystallize and to increase the bioactivity with respect to the original 45S5 composition.[15–17] In particular, some specific ions (such as copper, zinc, silver, strontium, and magnesium) have shown favorable effects in terms of biological response, and have been therefore named as "therapeutic ions."[17–20]

For example, magnesium is fundamental for bone metabolism, increases bone cell adhesion and stimulates new bone formation,[21] while strontium can be employed to stimulate osteogenesis and to reduce bone resorption in vivo, since it is able to stimulate osteoblasts and inhibit osteoclasts.[22] Many compositions containing such ions have been described in the literature and the effect of each single ion was investigated.[23]

Among others, the recently developed bioactive glass BGMS10 (see Table 1 for its chemical composition) showed a favorable combination of properties, that is, an extremely high crystallization temperature (≈932°C) coupled with a very good bioactivity and biocompatibility (confirmed also by means of an innovative 3D in vitro model with human mesenchymal stem cells). This BG resulted suitable for the preparation of a large variety of products, such as granules, scaffolds, dental putties, wound dressings, composite systems, and coatings.[24,25] Moreover, Bio_MS (Table 1), another composition containing strontium and magnesium, has revealed very promising features. In fact, such BG exhibited an outstanding biological performance, better than 45S5, together with a very high crystallization temperature and a large processing window, which permits to obtain completely amorphous products despite the possible thermal treatment.[26] The biological responsiveness of Bio_MS was evaluated employing bone marrow mesenchymal stem cells (BM-MSCs) and basing on an innovative in vitro model, which mimicked the real operating theater. BM-MSCs were able to colonize the material and undergo differentiation versus bone lineage, thus demonstrating the excellent regenerative potential of the novel BG. Bio_MS, due to its outstanding performance, was patented (Italian patent).

In this work, for the first time, the two novel bioactive glasses BGMS10 and Bio_MS were tested in vivo in an animal model, to confirm the excellent behavior outlined by the aforementioned in vitro tests. This constitutes an important step towards clinical trials. Both BGs were implanted bilaterally in the rabbits' femurs. To better evaluate the regeneration potential of these new materials, also the gold standard 45S5 was implanted with the same procedure.

2 | MATERIALS AND METHODS

2.1 | Bioactive glass granules preparation

The bioactive glasses BGMS10 and Bio_MS were designed and obtained by melt-quenching techniques, as described elsewhere.[24–26] In summary, the raw materials (from Carlo Erba, Italy) were melted in a platinum crucible in air at 1450°C (heating rate: 10°C/min). The molten glasses were then rapidly quenched in water and frits were obtained. The frits were left to dry at about 110°C for 16 h. The chemical compositions of the BGs are reported in Table 1.

The frits were then ground in alumina jars and subsequently sieved to obtain granules with proper granulometry (granular size between 100 and 500 μm) to be directly implanted. Such granules were sterilized by autoclave before surgery.

2.2 | In vitro assessment of cytocompatibility on granules

Preliminary to in vivo tests, BG granules were tested according to the ISO standard 10993-5 "Biological evaluation of medical devices-Part 5: Tests for in vitro cytotoxicity,"[27] to exclude any potential cytotoxicity.

The osteocyte-like murine long bone cell line (MLO-Y4) was selected for cytocompatibility tests (in accordance to the ISO standard 10993-5), since this line concerns the most represented cell type of bone, target tissue for the bioactive glasses here investigated.[28,29] The cell line was cultivated in Dulbecco's modified Eagle's medium (DMEM) (Euroclone, Milan, Italy) supplemented with 10% fetal bovine serum (Merck Life Group, Darmstadt, Germany) and 1% antibiotics (100 µg/mL pen-streptomycin) (Merck Life Group, Darmstadt, Germany). Serum-free DMEM was used as a negative control, while latex was used as a positive control. The same amount of latex weight (20, 40, and 60 mg) compared to granules was used for the Neutral Red test. Similarly to MTT assay, latex extracts were obtained by maintaining a ratio of 6 cm^2/mL between the area of the material and the culture medium, according to the ISO 10993-12 standard of the reference sample. Since many microorganisms showed optimal growth at 37°C, the eluate was filtered through a 0.22-µm filter as an additional safety procedure to ensure the elimination of potential microbial species.

Quantitative analyses for the two assays were performed with a spectrophotometer (Multiskan RE, Thermo Labsystem, Milan, Italy) at a wavelength of 540 nm for the Neutral Red and 570 nm for the MTT assay,[30–33] respectively.

2.2.1 | Morphological evaluations

Observation and evaluations of direct contact between BG granules (at different concentrations) and MLO-Y4 cells were performed after incubation (for 24 and 72 h), under a light microscope. This assessment was carried out before performing the NR uptake assay.

Microscopic observation included morphological signs that could indicate cellular suffering such as lysis, swelling, or intracytoplasmic thickening. Quantitative analysis by optical density (O.D.) gives a value of the cytotoxicity induced by the material, which is compared with the value of cells in contact with non-cytotoxic substances (DMEM without serum as a negative control).[34]

The morphology of the granules in contact with MLO-Y4 cells was also investigated by scanning electron microscopy (SEM) using a FEI Quanta 200 instrument (Fei Company, Eindhoven, The Netherlands), coupled to an INCA 350 EDS apparatus (Oxford Instruments, Abingdon, United Kingdom). After 24 h of incubation with the granules, the cells were rinsed with Dulbecco's phosphate buffer solution (DPBS), fixed in glutaraldehyde 2.5% (G5882-Sigma-Merck, Darmstadt, Germany), dehydrated with ascending ethanol scale, sputtered by 10 nm layer of gold and observed.[35]

2.2.2 | NR uptake

Neutral Red (NR) uptake (NR solution N2889 Sigma-Merck, Darmstadt, Germany) is a widely used test for cytotoxicity evaluation, applied to assess the number of viable cells in a culture.[36] NR is a vital dye which accumulates in lysosomes of viable cells in culture. Cytotoxicity of a material is estimated as a reduction in the NR uptake into the cell after given periods of time of direct exposure to the material itself.

Cells (1.5×10^5/mL DMEM) were seeded and cultured for 24 and 72 h. For each well, different concentrations of granules were added (20, 40, and 60 mg/mL) and incubated at 37°C ± 1°C, 90% ± 5% humidity and 5.0% ± 1% CO^2/air. At the end of the incubation, 150 µL of NR solution was added to each well and placed in the incubator for 3 h. Subsequently, the NR solution was discarded and MLO-Y4 cells rinsed with 150 µL DPBS. Ethanol/acetic acid mixture (150 µL) was added to each well to extract the NR dye from the cells, which was subsequently measured with a spectrophotometer (Multiscan RC by Thermolab, Thermo Fisher Scientific, Helsinki, Finland) at 540 nm to quantify the extracted solution. All experiments were replicated three times for each sample, adopting DMEM without serum (CTRL−) and latex (CTRL+) as terms of reference.

2.2.3 | MTT assay

MTT is a widely used colorimetric assay based on the cleavage of a yellow tetrazolium salt to form purple formazan crystals, as a consequence of mitochondrial enzymes in cells which are metabolic-active. It is utilized to estimate indirect toxicity and cell viability by spectrophotometry. Briefly, BG granules were added to the wells containing MLOY4 cells at a density 1×10^4 cells and incubated for 24 and 72 h. At the end of the incubation, 10 µL per well of MTT reagent prepared in D-PBS were then added to each well and incubated at 37°C for 4 h. A quantity of 100 µL of Dimethyl Sulfoxide (DMSO) was added to each well and incubated at room temperature for 20 min, then the solubilized formazan was quantified at 570 nm on an ELISA plate reader. As previously described, DMEM without serum and latex were used as references (CTRL− and CTRL+, respectively). The sample extract was carried out in centrifuge tubes with a ratio between sample and extracting solution (DMEM without fetal bovine serum) according to ISO 10993-5.

2.3 | In vivo tests

2.3.1 | Animals and surgery

The scientific literature demonstrates that rabbits are suitable as animal models for bone implants, because they show a similar bone density to humans and a higher bone remodeling rate than humans: thus, faster results and at a lower cost can be collected.[37,38] Even if large animal models are more similar to humans in bone healing mechanisms, the European Communities Council Directive recommends excluding large animal models (such as dog, sheep and pork) on an ethical basis, whether a small animal can be effective for the research purpose.[39] For these reasons, a total of 15 healthy white New Zealand rabbits (Harlan Laboratories S.r.l, Correzzana, Monza e Brianza, Italy), with an average body weight of 5 kg, were employed.

Experiments were conducted in compliance with the Bioethical Committee of the Italian National Institute of Health and licensed with Decrees of the Italian Ministry of Health (Protocol Number: 210/2013-B). Animal maintenance, care and surgery were performed in conformity with Italian law (D.L. No. 26/2014) and European regulation (EEC No. 63/2010).

For surgery, general anesthesia was induced by a mixture of ketamine (30 mg/kg body weight—Imalgene 1000, Merial Italia S.p.A., Milano, Italy) and xylazine (4 mg/kg body weight—Sedaxylan, Dechra Veterinary Products S.r.l., Torino, Italy). An additional sedation was achieved whether necessary through propofol (7 mg/kg—Propovet, Ecuphar S.r.l., Piacenza, Italy) administered in the marginal ear vein. Shaving and antisepsis were accomplished on the lower limbs to be operated, afterwards induction of anesthesia. A 3 cm long skin incision was accomplished to the lateral skin of the distal femur, and blunt muscles were dissected to expose the distal femur lateral condyle. Implant site preparations were performed using a Piezosurgery® unit with insert tip IM4A (Mectron, Carasco, Genova, Italy) and irrigation with sterile saline as coolant. So, by means of this handy and precise osteotome,[40–42] a regular and repeatable hole or bone void, 5 mm in diameter and 10 mm in depth (representing a "critical size defect"), was obtained. Only one femur implant (i.e., BG material) per side was placed in each animal as shown in Tables 2 and 3. After materials' implantation, the surgical flaps were closed in layers and sutured by 4.0 glycolide/L-lactide copolymer (Vicryl®, Ethicon, Johnson & Johnson Spa, Pomezia, Rome, Italy) and the skin with 3.0 silk (Perma-hand® Silk Suture, Ethicon, Johnson & Johnson Spa, Pomezia, Rome, Italy). The sutured area was treated with iodine to prevent post-surgical infection. Antibiotic (Baytril®, Bayer, Italy) was administered intramuscularly for 3 days (enrofloxacin, 10 mg/kg body weight—Baytril® 5%, 50 mg/mL, Bayer S.p.A., Milan, Italy) and analgesic treatments (buprenorphine, 0.05 mg/kg body weight—Temgesic®, Indivior Italia S.r.l., Milan, Italy) were given. The animals were housed with veterinary care and nutritional supplement in singular cages during the whole laboratory period.

Implanted rabbits were divided in two groups according to two different times of euthanasia after the implantation surgery: at 30 days (hereinafter referred to as "short-term implantation group") and at 60 days (hereinafter referred to as "long-term implantation group"). Generally, all the rabbits were euthanized after surgery by intravenous injection of embutramide/mebezonium iodide (0.3 mL/kg body weight—Tanax 50 mg, MSD Animal Health S.r.l. Italia, Segrate MI, Italy) under general anesthesia with a mixture of xylazine (4 mg/kg body weight—Sedaxylan®, Dechra Veterinary Products Srl, Turin, Italy) and ketamine (30 mg/kg body weight—Imalgene 1000®, Merial Italia SpA, Milan, Italy). The disarticulated femurs were fixed in buffered formaldehyde, as specified in the next paragraph.

TABLE 2 BG granules implantation in rabbits' left and right femurs.

	Left femur (BG)	Right femur (BG)
1	BGMS10	45S5
2	BGMS10	BGMS10
3	Bio_MS	Bio_MS
4	Bio_MS	45S5
5	Bio_MS	45S5
6	BGMS10	45S5

Note: Short-term study group (animals sacrificed 30 days after implant surgery).

TABLE 3 BG granules implantation in rabbits' left and right femurs.

	Left femur (BG)	Right femur (BG)
1	BGMS10	45S5
2	BGMS10	45S5
3	BGMS10	BGMS10
4	Bio_MS	Bio_MS
5	Bio_MS	Bio_MS
6	Bio_MS	45S5
7	Bio_MS	45S5
8	BGMS10	45S5
9	BGMS10	45S5

Note: Long-term study group (animals sacrificed 60 days after implant surgery).

2.3.2 | Short-term study (rabbits sacrificed 30 days after implant surgery)

Six rabbits were used: considering two femurs per animal ($n = 12$), four samples for each type of bioactive glass (45S5, BGMS10, and Bio_MS granules respectively) were obtained, as reported in Table 2.

2.3.3 | Long-term study (sacrificed 60 days after implant surgery)

Nine rabbits were used: considering two femurs per animal ($n = 18$), six samples for each type of bioactive glass (45S5, BGMS10, and Bio_MS granules respectively) were considered, as reported in Table 3.

2.4 | Histomorphometry (scanning electron microscopy) and histology (light microscopy)

The femoral distal epiphyses were fixed in buffered formaldehyde, pH 7.4 for 4 days. Then, they were dehydrated in a graded series of ethanol and embedded in polymethylmethacrylate. The specimens were serially sectioned (300 μm in thickness) in a plane perpendicular to the longitudinal axis of the femurs, with a Leica SP 1600 diamond

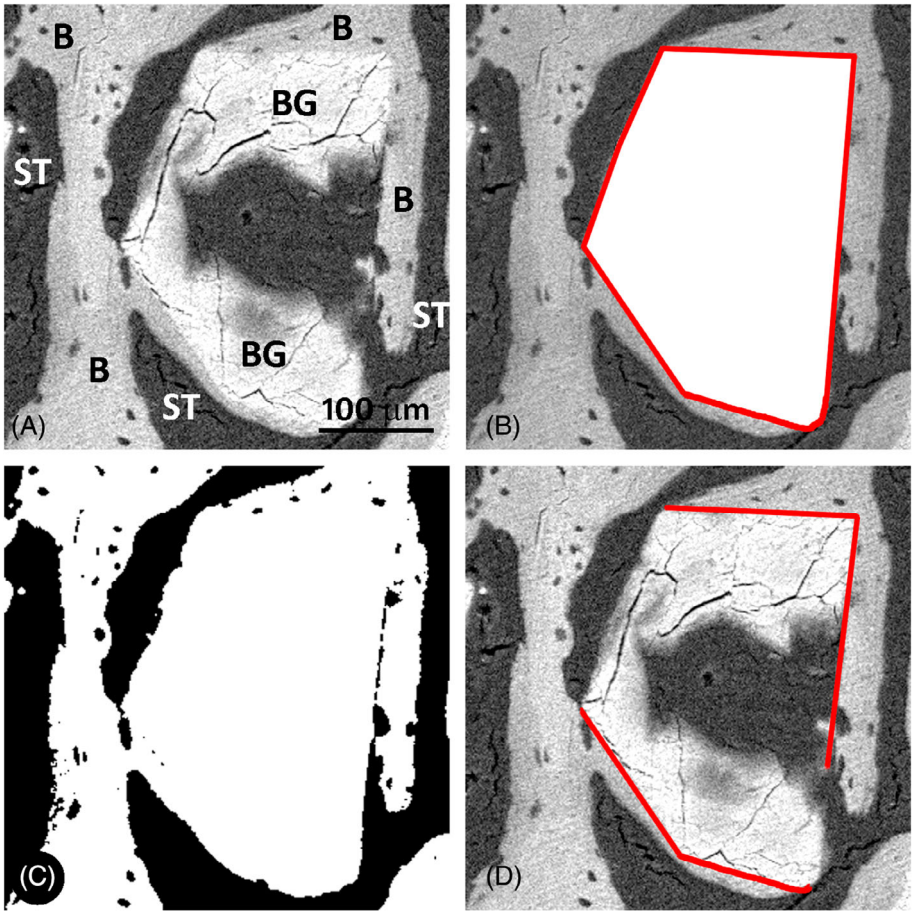

FIGURE 1 (A) Detail of SEM micrograph showing how measurements were performed; B, bone; BG, bioactive glass granule; ST, soft tissue. (B) Each BG was manually outlined (red line) and filled with white color to obtain, respectively, its perimeter and area. (C) Bone and BGs were selected with the threshold function and binarized in white color, while soft tissue resulted black. (D) The perimeter of BGs in contact with bone was outlined (red lines) to calculate the affinity index.

saw microtome (Leica SpA, Milan, Italy) cutting system under water irrigation. For each specimen, the section corresponding to the center of the drilled hole containing the BG was selected under optical microscope (Eclipse Ni-E, Nikon) and sputter-coated with an 8–10 nm gold–palladium layer (Emitech K550, Emitech Ltd, Ashford, Kent, UK) for Scanning Electron Microscope (SEM) analysis. Samples were observed with a SEM (SEM-QUANTA 200, FEI Company, the Netherlands) under low vacuum, using the backscatter mode at 100× magnification. The SEM was equipped with energy dispersion X-ray spectroscopy (EDS, Inca, Oxford Instruments, UK) and was used also to acquire elemental maps.

Each digital image was saved and analyzed by means of the ImageJ software for histomorphometry. A square Region of Interest (ROI) of $2 \times 2\ mm^2$ was selected and the relative area occupied by BGs (BG area), bone (B area) and soft tissue (ST area) were calculated. Briefly, each BG granule was manually outlined and filled with white color to obtain its area and perimeter (Figure 1, in particular Figure 1B). With the threshold function, the bone and the BGs were selected and binarized in white color, while soft tissue resulted black (Figure 1C). The affinity index (AI), defined as the perimeter of BG granules in contact with bone over the BG total perimeter, was calculated (Figure 1D). Moreover, the trabecular thickness (Tb Th) was evaluated manually measuring in 40 random points the thickness of the trabeculae present in the ROI.

Histological analysis was performed under light microscope—LM (Eclipse Ni-E, Nikon): the sections adjacent to that used for SEM analysis were glued to a microscope slide, thinned with fine grain emery papers, and polished with alumina. A superficial staining was performed with an alcoholic solution of toluidine blue (2 min at 60°C), then rinsed with tap water; a few drops of HCl 0.1 N solution were added on top of the section for 30 s and rinsed; finally, a few drops of an alcoholic solution of basic fuchsin were added for 30 s and rinsed.

2.5 | Statistical analysis

For in vitro tests, all results were statistically treated using ANOVA test followed by Dunnett's multiple comparison test analysis. GraphPad Prism8 software for Windows was used to perform the analysis and drawing of the graphs.

Histomorphometric data were compared among groups for the same time point using the ANOVA test followed by Bonferroni's post hoc analysis; comparison between the same group at 30 and 60 days was performed with the Student's *t* test. All values were expressed as the mean ± standard deviation. Stata 11 (StataCorp LLC, College Station, TX) software was used for the analysis. A p value <.05 was considered statistically significant.

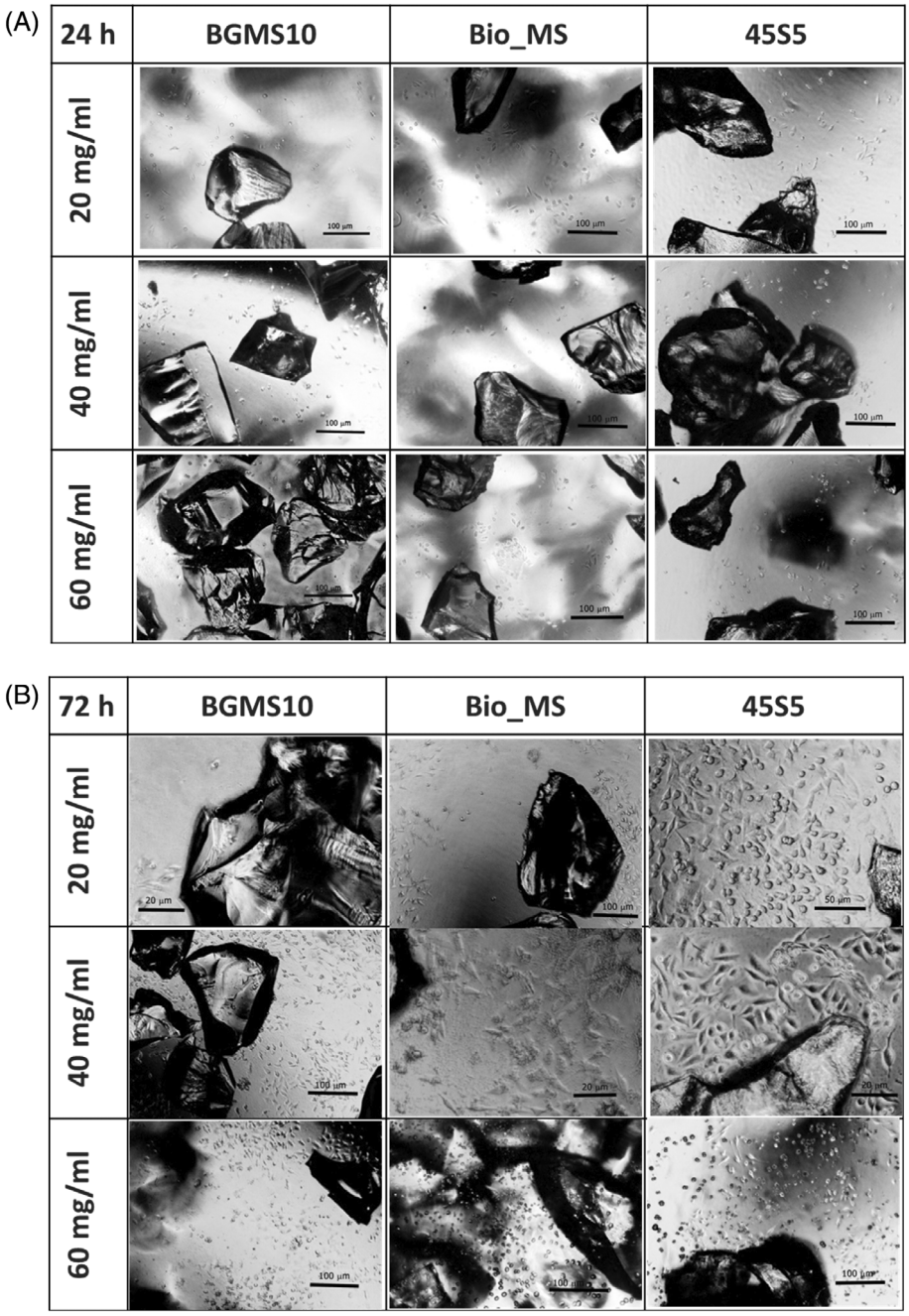

FIGURE 2 Optical microscopy images of BGMS10, Bio_MS and 45S5 granules after 24 h (A) and 72 h (B) of MLO-Y4 cells incubation in DMEM at 37°C. No significant change in cellular morphology (such as lysing and rounding) was observed.

3 | RESULTS

3.1 | In vitro tests

The morphological evaluation of MLO-Y4 cells, 24 and 72 h after positioning BGs in culture medium, was studied by light microscopy, as shown in Figure 2. The cells were placed in contact with different amounts (20, 40, and 60 mg/mL) of bioactive glasses' granules to verify the dose-dependent level of cytotoxicity. There were no signs of cellular intolerance such as lysis, intracytoplasmic thickening, or membrane alterations at any of the BGs granules concentrations inside the cell cultures. After 24 h any level of toxicity was not recorded at any of the concentrations introduced. After 72 h the situation did not change in terms of cytotoxicity, but an increased cell proliferation was detected with no significant difference between the two samples (BGMS10 and Bio_MS), at any concentration as well.

To confirm the cytocompatibility of the glasses in contact with the cells for 24 h, SEM images were acquired and showed, in presence of BGs, an optimal MLO-Y4 cell morphology and good cell proliferation (Figure 3). No cellular suffering state, such as lysis, swelling, or intracytoplasmic thickening, was evidenced.

On the contrary, a positive stimulation of cell proliferation was observed, probably related to the gradual degradation of bioactive molecules, in particular 72 h after cell culture in presence of BG

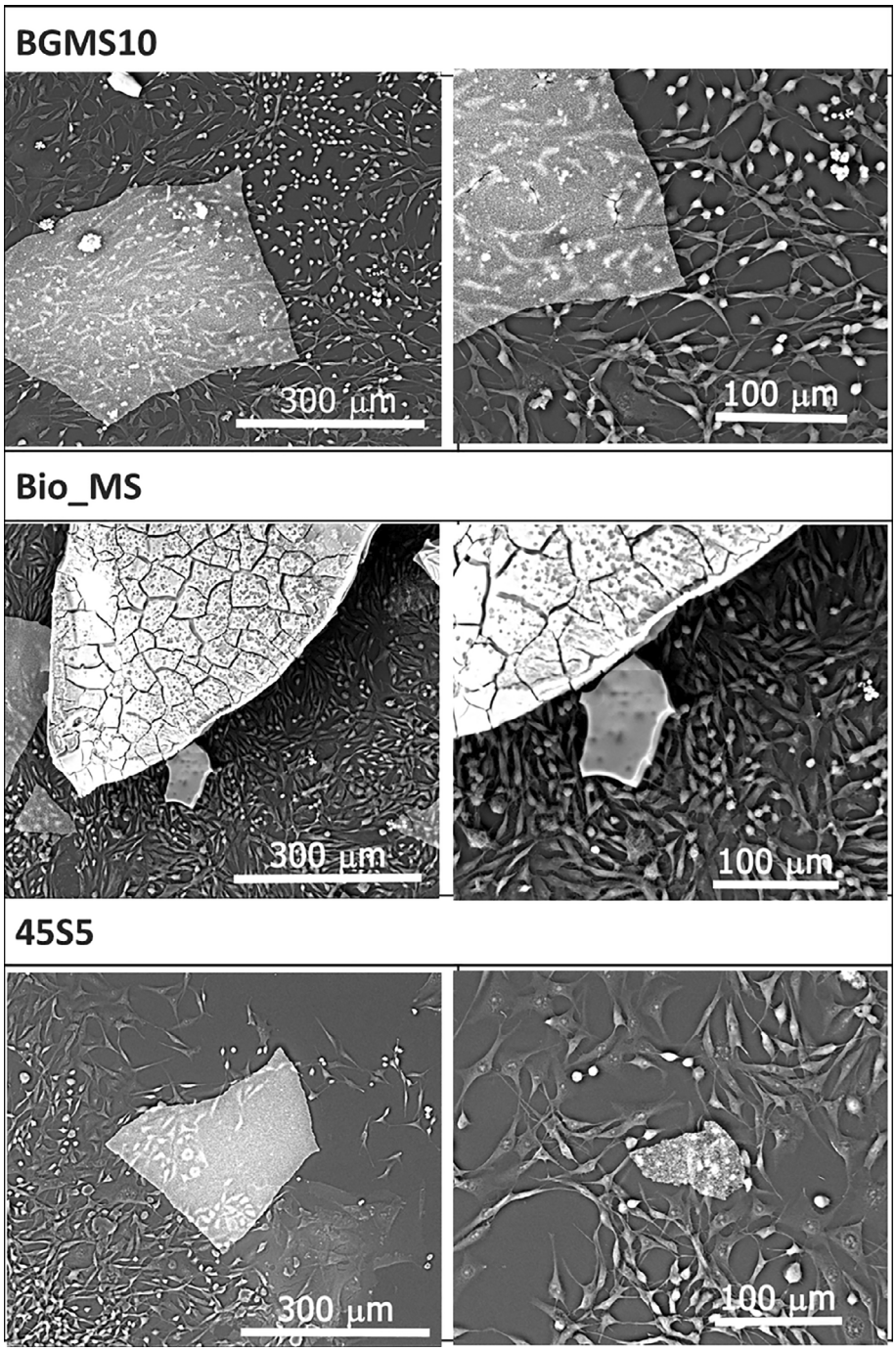

FIGURE 3 SEM images of BGMS10, Bio_MS and 45S5 granules after 24 h of MLO-Y4 cells incubation in DMEM at 37°C. The images at higher magnification (right side) show representative granules colonized/surrounded by adherent cells (MLO-Y4). Cells show unchanged morphology, with flat, oval nucleus and their typical spindle-shaped cytoplasm.

granules into the well (i.e., NR uptake). The NR uptake assay indeed evaluates the ability of viable cells to incorporate and store the neutral red dye within their lysosomes. Due to a hypothetical toxic action of the materials object of the assessment, alterations of the lysosomal membrane may occur, resulting in reduced/absent intracytoplasmic accumulation of the dye. In this process, viable cells are distinguished from damaged or dead cells.[43]

NR uptake after 24 h showed a better result of BGMS10 (60 mg) compared to the reference material 45S5 (60 mg). The test results read after 72 h revealed a higher O.D. of BGMS10 (40 mg) with respect to 45S5 (40 mg) (Figure 4). Moreover, no significant alteration in lysosomal activity ascribed to cytotoxic effects of the samples at all different concentrations was noticed.

Cytocompatibility was further quantitatively assessed on eluates from the samples, using International Standards Organization (ISO) requirements for eluate preparation and cytotoxicity assessment.[27] The MTT assay was applied, to assess possible damage at the mitochondrial level.[44–46] The MTT assay results (Figure 5) demonstrated samples with an excellent viability performance at 24 and 72 h, that is, without induction of damage to the

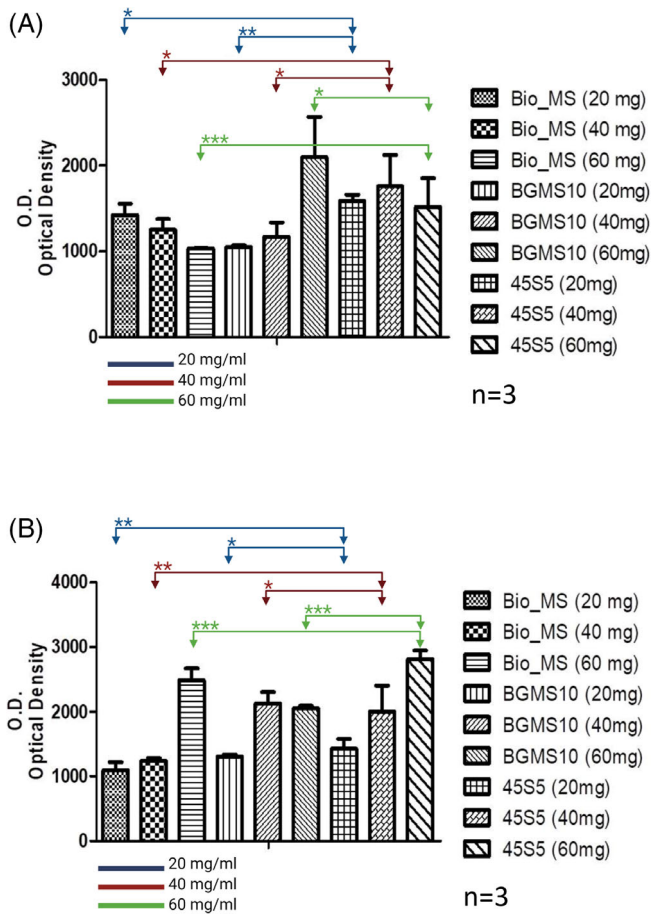

FIGURE 4 (A) Cellular viability (NR uptake 24 h) of MLO-Y4 cells after incubation with Bio_MS, BGMS10, and 45S5 at different concentrations (20, 40, and 60 mg/mL). (B) NR uptake 72 h of MLO-Y4 cells after incubation with Bio_MS, BGMS10, and 45S5 at different concentrations (20, 40, and 60 mg/mL). Statistical analysis was completed using one-way ANOVA followed by Dunnett's test (***$p \leq .001$; **$p \leq .01$; *$p < .05$). The number of replicates (n) is equal to 3.

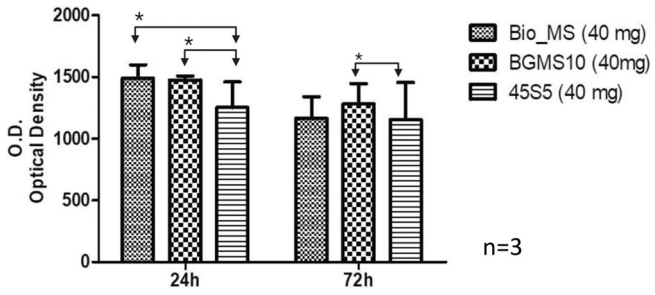

FIGURE 5 MTT test performed on MLO-Y4 cells after 24 and 72 h of incubation with Bio_MS, BGMS10 and 45S5 eluates. Statistical analysis was completed using one-way ANOVA followed by Dunnett's test (*$p < .05$). The number of replicates (n) is equal to 3.

mitochondrial activity of MLO-Y4 cells. In particular, Bio_MS and BGMS10 demonstrated a better O.D. compared to 45S5 both at 24 and 72 h.

3.2 | SEM analysis and histomorphometry

The morphological appearance of sections examined under SEM (Figure 6) is very similar among the three groups at 30 days. In fact, in all the groups, there are numerous BG granules of various sizes and shapes that appear largely surrounded by thin bone trabeculae. The dark areas, representing soft tissue, seem evenly distributed among bone and granules in all groups. At 60 days, on the contrary, only the 45S5 group shows a different morphological aspect with respect to both the other two groups at 60 days and to all groups at 30 days; in fact, it shows large amounts of soft tissue and few scattered BG granules, surrounded by wide bone trabeculae, that appear less abundant compared to all other groups. The appearance of the BG granules varies considerably between 30 and 60 days in all groups. In fact, while at 30 days the granules have well-defined contours with many sharp corners and are almost completely surrounded by a thin layer of bone, at 60 days the morphology of granules is more heterogeneous among the three groups, and granules appear less surrounded by bone. In particular, only in the 45S5 group, BG granules appear less abundant and with more rounded aspect than the other two groups, whose contours are not well defined due to dark areas inside the granules that prevent them from clearly defining their perimeters (Figure 7).

The bioactive bone-bonding mechanism and the formation of new bone tissue were further investigated by means of X-ray microanalysis. Figures 8 and 9 show the results relative to some sections of the BGMS10 and the 45S5 groups at 30 and 60 days, which are particularly representative as they show the typical reaction stages of bioactive implants in biological environment; the results of the Bio_MS investigation are similar to those of the BGMS10, therefore they are not shown for the sake of brevity. As widely reported by the literature,[47,48] a common characteristic of BG granules is their time-dependent dissolution, with concomitant formation of a biologically active hydroxyapatite (HA) layer on their surface; HA is a mineral phase structurally and chemically analogous to that of bone and provides the bonding interface with tissues. According to the protocol developed by Hench and coworkers,[47,48] the HA formation is preceded and accompanied by a rapid release of alkaline ions and a loss of soluble silica from the glass surface, due to the breaking of the Si—O—Si bonds, which leads to the formation of a silica gel layer (sg). The formation of sg has been observed in all the investigated samples and it is reported, as an example, in Figures 8 and 9 for BGMS10 and 45S5 glasses. In addition, while after 30 days it is possible to observe several glass granules which have been partially dissolved by the physiological environment (particularly for the BGMS10 and Bio_MS group: see Figure 8A,E), after 60 days most of the glass has almost completed the reaction process, thus transforming into HA or into areas rich in silica gel and calcium phosphate; few isolated glass formations are surrounded by sg or HA. This fact is further demonstrated by the results of the EDS maps in Figure 8E,F, where Si is representative of both the glass and the silica gel, while Ca is representative of both HA/calcium phosphate and bone tissue; in particular, the glass appears lighter than the sg with the backscattered detector of SEM (i.e., electron-opaque), while the bone has a typical morphology, very

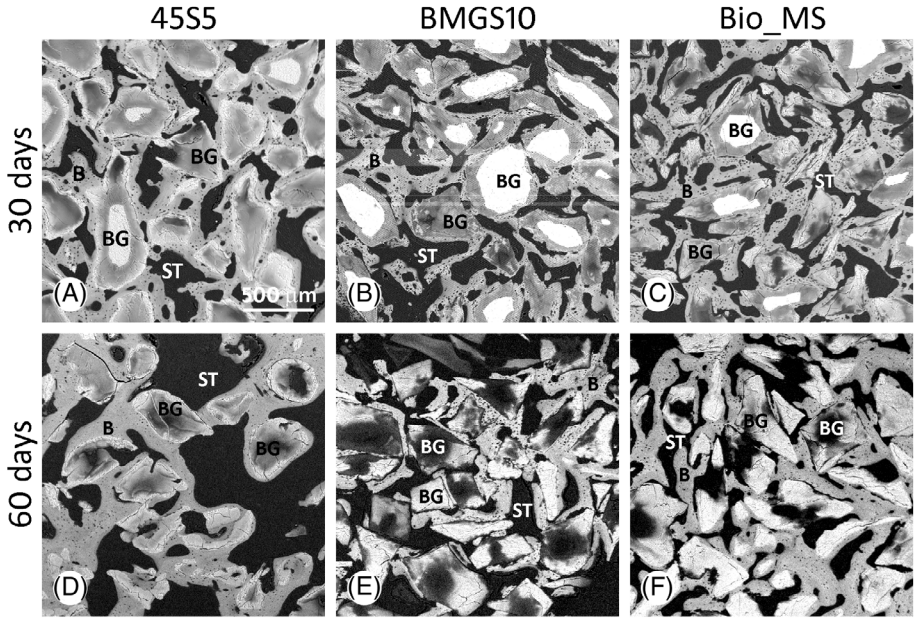

FIGURE 6 SEM representative micrographs showing the morphological aspect of sections examined for each group (45S5, BGMS10 and Bio_MS) at 30 ($n = 12$) and 60 days ($n = 18$). Note the similar morphological appearance in all groups, except in the 45S5-60 days group. In fact, this group shows wider bone trabeculae (B), large amounts of soft tissue (ST) and less bioglass granules (BG) with respect to all other groups, where numerous BG granules appear of various sizes and shapes, and largely surrounded by thin bone trabeculae.

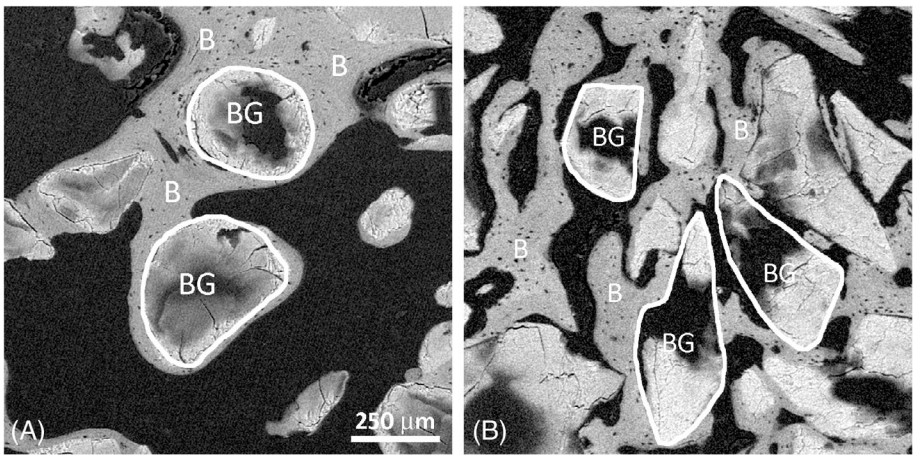

FIGURE 7 Detail of SEM micrographs. (A) Morphological aspect of a section of the 45S5 group at 60 days: note the wide bone trabeculae (B) and bioglass granules (BG) with a rounded outline. (B) Morphological aspect of a section of the BGMS10 group at 60 days (similar to Bio_MS): note the thin bone trabeculae (B) and bioglass granules (BG) whose aspects are not well defined due to dark areas inside the granules that prevent clearly defining their perimeters. White lines highlight the contour of some bioglass granules.

different from that of HA. Regarding the 45S5, already after 30 days it is less frequent to observe the presence of residual glass granules, as most of the implanted glass has been converted into silica gel and HA, which in SEM micrographs appears as a lighter region surrounding what remains of the granules (Figure 9).

Results from histomorphometric analysis, in line with the morphological appearance, are reported in Table 4. Regarding the bioglass area (BG area), short-term (30 days) data show no significant differences among the 45S5, BGMS10 and Bio_MS groups, while at 60 days the average bioglass area is smaller in the 45S5 group with respect to the two others (significant only vs. Bio_MS group). Long term (60 days) data show that only the 45S5 group has a significantly reduced BG area compared to 30 days, while in BGMS10 and Bio_MS groups the values do not change significantly during time. With regard to the bone area (B area), no significant differences were found among the three groups at both 30 and 60 days; moreover, no significant variations are present for each group between 30 and 60 days. The trabecular thickness (Tb Th) does not change significantly among groups at 30 days, while increases significantly at 60 days with respect to 30 days within each group. At 60 days in the 45S5 group the Tb Th is higher than novel BGs (significantly only vs. the Bio_MS group). The area of soft tissue (ST area) did not differ quantitatively among the three groups at 30 days, while at 60 days the amount of soft tissue is significantly higher in the 45S5 group with respect to the BGMS10 and Bio_MS groups. Long term (60 days) data show that only the 45S5 group has a significantly increased ST area compared to 30 days, while in BGMS10 and Bio_MS groups it does not change significantly. Regarding the affinity index (AI), no significant differences were found among the three groups at both 30 and 60 days. On the other hand, in each group, AI value is always significantly lower at 60 days with respect to 30 days.

3.3 | Light microscopy (LM) analysis

In all groups of the short term study, LM observations (Figure 10) show that the new bone trabeculae are formed by intramembranous ossification, both inside the soft tissue and directly in contact with BG

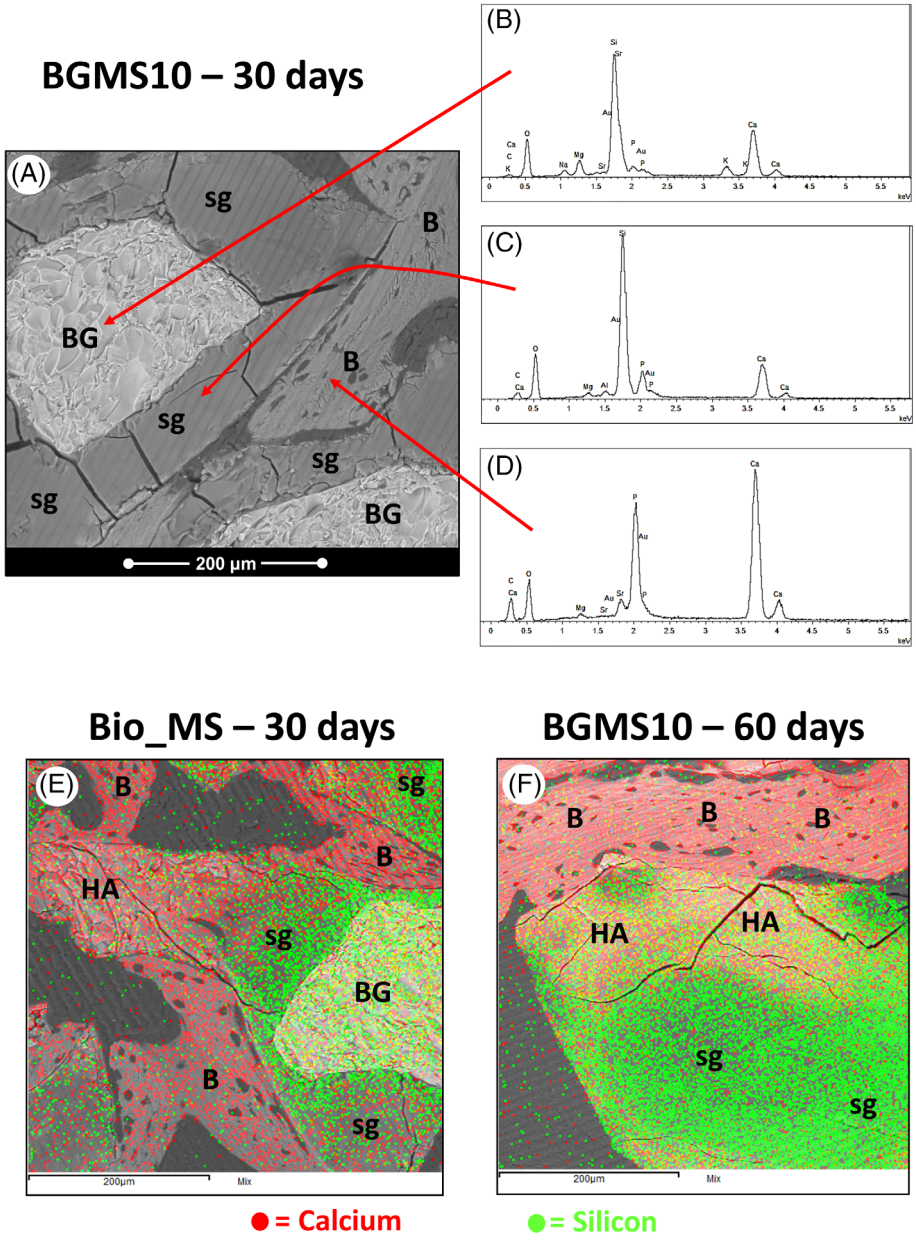

FIGURE 8 BGMS10 group at 30 and 60 days: representative SEM micrographs and results of the X-ray microanalysis (B–D). In particular, (E and F) report the X-EDS maps showing the distribution of Si—representative of both the glass and the silica gel—and Ca—representative of both the hydroxyapatite (or the calcium phosphate rich phase) and the bone tissue—in the BGMS10 group. B, bone; BG, bioactive glass; HA, hydroxyapatite; sg, silica gel.

granules. Two are the relevant features: (i) most osteocyte lacunae inside the bone trabeculae are filled by large and roundish osteocytes, typical of static osteogenesis (see discussion); (ii) bone surfaces are mainly lined with osteoblastic laminae, clearly visible, involved in deposition of the osteoid seams.

In the long term study (Figures 11 and 12), bone trabeculae surrounding BG granules show signs of bone remodeling, characterized by the presence of well-defined reversal lines, interposed between primary and secondary bone. Relevant features are: (i) primary bone is characterized mainly by numerous and large lacunae containing roundish osteocytes, as observed in the short term study, while secondary bone shows small lacunae containing almond-like shaped osteocytes (see discussion); (ii) numerous osteoblastic laminae are present on the bone surfaces and some osteoclasts are detectable both close to some bone trabeculae and BG granules.

4 | DISCUSSION

This preliminary study investigated whether and how the two novel bioglasses (BGMS10 and Bio_MS), implanted in rabbits' femurs, can improve and support the healing process of osseous defects, compared to the gold standard bioglass (45S5).

Preliminary in vitro tests, performed to assess the cytocompatibility on new BG granules, pointed out the good cell adhesion around the samples after only 24 h of contact. NR uptake and MTT assay quantitative results were confirmed from a morphological point of view by both the observations under the optical and electron scanning microscope. Abiraman et al.[49] had in the same way observed at SEM that the bioactive glasses seeded with fibroblasts (L929) led to a change in pH following the dissolution and precipitation of the calcium phosphate complex, which contributed to cell

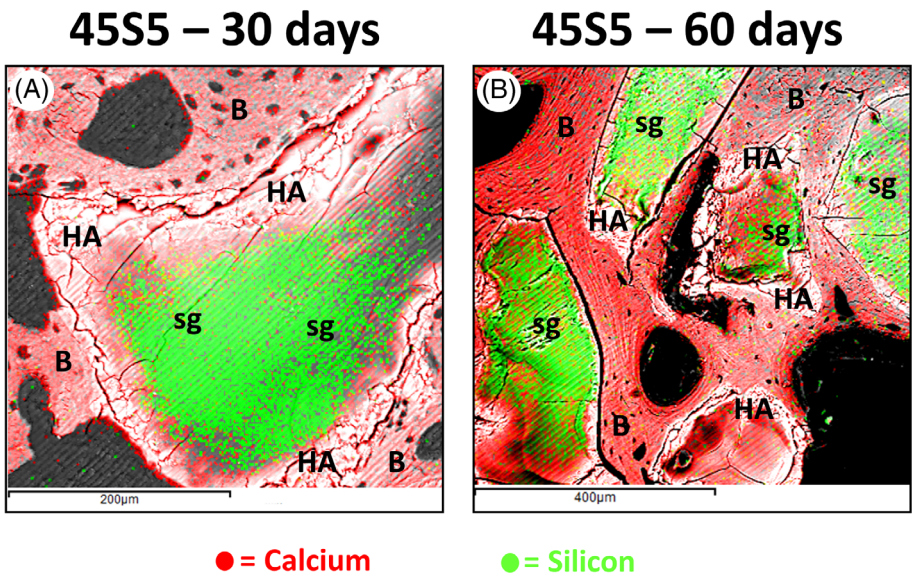

FIGURE 9 45S5 group at 30 (A) and 60 (B): representative SEM micrographs and X-EDS maps showing the distribution of Si—representative of both the glass and the silica gel—and Ca—representative of both the hydroxyapatite (or the calcium phosphate rich phase) and the bone tissue. B, bone; BG, bioactive glass; HA, hydroxyapatite; sg, silica gel.

TABLE 4 Area of bioglasses (BG area), area of bone (B area), trabecular thickness (Tb Th), area of soft tissue (ST area) and affinity index (AI) in rabbits implanted with 45S5, BGMS10 and Bio_MS bioglasses for 30 ($n = 12$) and 60 days ($n = 18$).

	45S5	BGMS10	Bio_MS
BG area 30 days	41.3 ± 5.1	38.4 ± 2.3	45 ± 6.3
BG area 60 days	26.5 ± 4.5* versus Bio_MS 60 days versus 45S5 30 days	37 ± 8.8	41.5 ± 11.2
B area 30 days	32.5 ± 4.5	24.1 ± 2.9	29.9 ± 1.8
B area 60 days	29.9 ± 4.9	31.7 ± 7.1	30.8 ± 7.9
Tb Th 30 days	71.2 ± 3.3	68.8 ± 4	69 ± 2.6
Tb Th 60 days	117.2 ± 18.4* versus Bio_MS 60 days versus 45S5 30 days	96.2 ± 16.9* versus BGMS10 30 days	90.8 ± 13.4* versus Bio_MS 30 days
ST area 30 days	26.5 ± 4.9	28.4 ± 6.6	25.4 ± 4.3
ST area 60 days	46.6 ± 4.1* versus BGMS10 60 days versus Bio_MS 60 days versus 45S5 30 days	31.1 ± 5	27.6 ± 5.6
AI 30 days	88 ± 7.6	74.8 ± 12.2	79.8 ± 5.4
AI 60 days	63.1 ± 14.4* versus 45S5 30 days	56.3 ± 6.6* versus BGMS10 30 days	52.1 ± 12.4* versus Bio_MS 30 days

Note: All values are expressed as mean ± SD.
*$p < .05$; *t*-test between 30 and 60 days; ANOVA test among 45S5, BGMS10 and Bio_MS.

attachment and cell proliferation of fibroblasts.[50] From the results of this study, the bioactive glasses Bio_MS and BGMS10 showed good cytocompatibility.

In short term in vivo study (30 days) the histomorphometric and morphological results indicate that the osteoconductive properties of the novel BGs have similar performance compared to 45S5. In fact, in all groups, the amount of new bone and the area occupied by BG granules, as well as the aspect and thickness of new bone trabeculae and the affinity index, are similar (Figure 6 and Table 4).

In contrast, in long term in vivo study (60 days), various differences were observed as far as the performance of the new BGs are concerned, compared with the gold standard. In BGMS10 and Bio_MS groups the trabeculae are thin and uniformly distributed around many BG granules, while in the 45S5 group few BG granules are mainly surrounded by wide and scattered bone trabeculae, separated by large amounts of soft tissue (Figure 6 and Table 4). It is important to underline that, despite the bone trabeculae being wider in the 45S5 group, the amount of bone area is similar to all other groups, not only at 60 days but also at 30 days: what changes is the spatial distribution of the bone trabeculae. In fact, in the 45S5 group, the redistribution of the bone trabeculae and consequently of the soft tissue is probably due to the reduction in the number of BG granules, due to their dissolution (Table 4). Moreover, on the basis of the histomorphometric data, it is possible to hypothesize the simultaneous reabsorption of some trabeculae (close to the site of dissolution of granules) along with the thickening of those remaining in contact with the undissolved granules. In particular, at 30 days in the 45S5 group, all BG granules are surrounded by thin trabeculae (as confirmed also by the

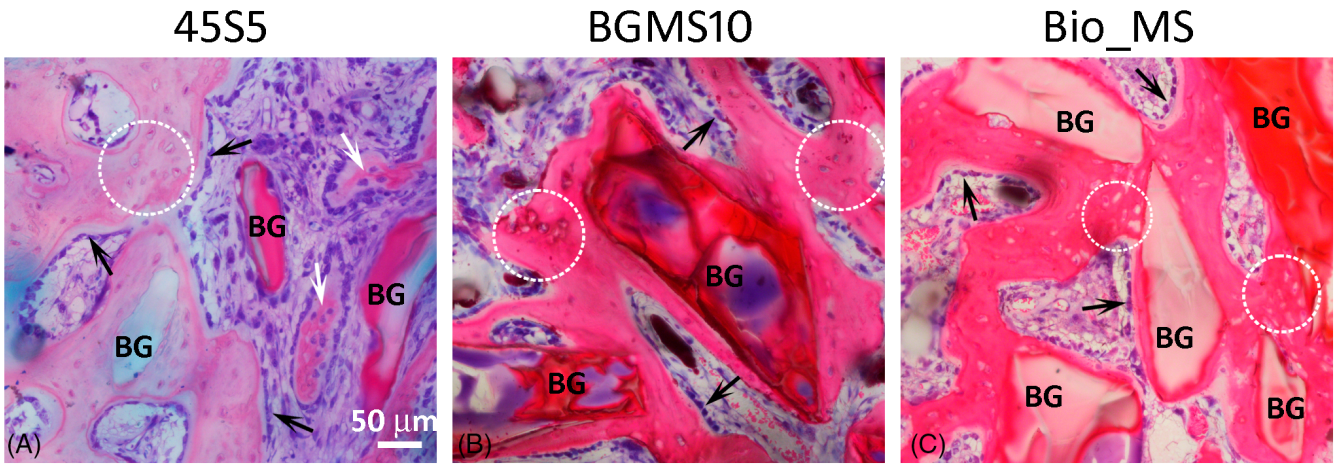

FIGURE 10 LM representative micrographs showing the morphological features of sections examined for each group (45S5, BGMS10 and Bio_MS) at 30 days ($n = 12$). Note the new bone trabeculae (white arrows) formed by intramembranous ossification both inside the soft tissue and directly in contact with bioglass granules (BG). Most osteocyte lacunae contain large and roundish osteocytes (white circles). Osteoblast laminae (black arrows) are clearly visible along many bone surfaces.

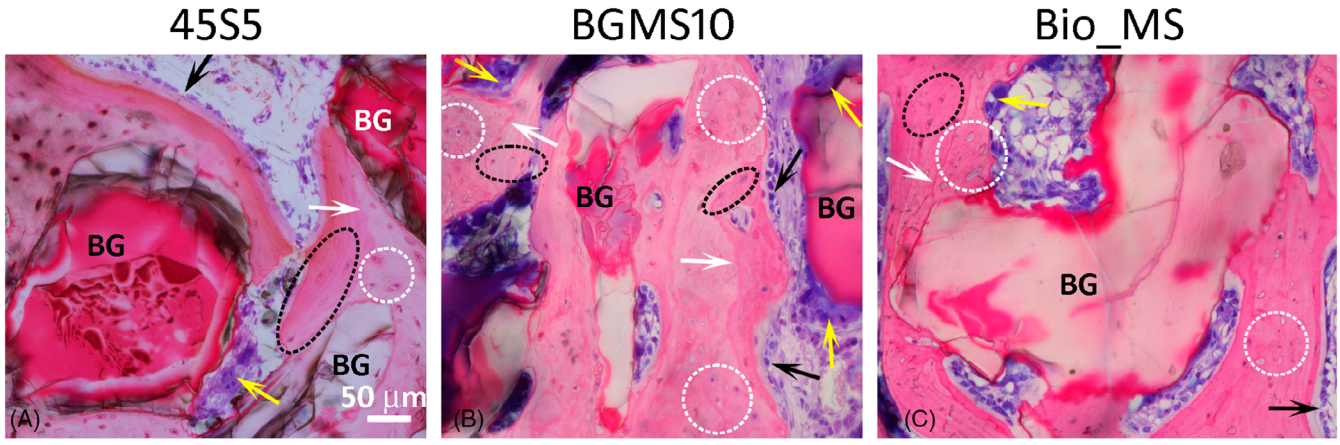

FIGURE 11 LM representative micrographs showing the morphological features of sections examined for each group (45S5, BGMS10 and Bio_MS) at 60 days ($n = 18$). Note the bone trabeculae showing reversal lines (white arrows). Primary bone with large and roundish osteocyte lacunae (white circles) and secondary bone with almond-like shaped osteocyte lacunae (black oval). Osteoblast laminae (black arrows) and osteoclasts (yellow arrows) are detectable both close to some bone trabeculae and bioglass granules (BG).

high Affinity Index, Table 4), but over time (between 30 and 60 days) some granules might be dissolved by biological liquids due to their high solubility[4,5] and/or be reabsorbed by osteoclast-like cells (Figure 11—45S5). This fast disappearance of some BG granules could prevent/decrease new osteogenesis and/or lead to the resorption of some thin trabeculae close to them, leaving wide areas of soft tissue. High solubility of these 45S5 granules could also explain their mostly rounded outline compared to all other groups (Figure 7). At the same time, the few undissolved 45S5 granules are surrounded by fewer but thicker trabeculae with respect to those present in the other groups. This result probably depends on the skeletal homeostasis that responds in the most appropriate way to the mechanical load[51,52]: in other words, in the 45S5 group the fewer and thicker bone trabeculae are supposed to bear the same mechanical load as the numerous and thinner trabeculae in the other two groups, since the value of bone area is the same in all groups. Although these results are preliminary and will need to be confirmed by further investigations, the condition observed in the novel BG groups (i.e., the presence of thinner and uniformly distributed bone trabeculae surrounding both a wider area of BG granules—that have not dissolved—and a lesser extent of soft tissue) could be advantageous. In other words, from the mechanical viewpoint, the features of novel BG granules allow for the neoformation of uniformly distributed bone trabeculae, compared to the less uniform coarse trabeculae, separated by large areas of soft tissue, induced by gold standard 45S5 granules.

Another point to be discussed is the fact that the trabecular bone area does not change quantitatively between 30 and 60 days in all groups, but it changes from the qualitative point of view. In fact, at 60 days the presence of cementing lines and the increase in trabecular thickness (especially in the 45S5 group) clearly indicate the

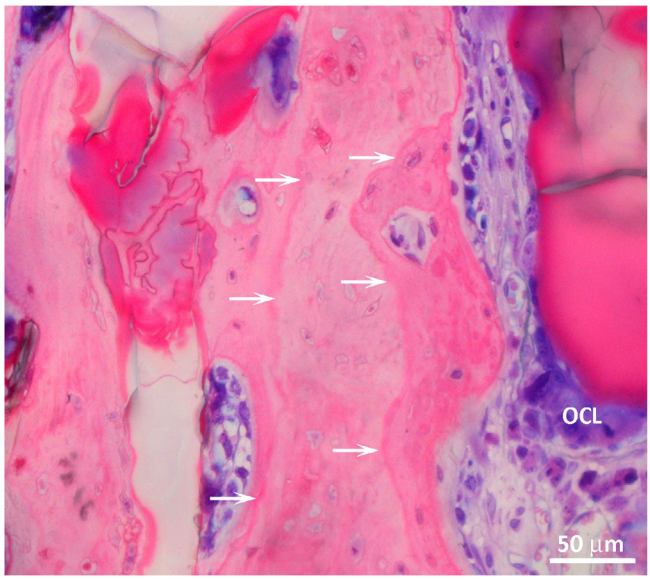

FIGURE 12 Detail of BGMS10 from section in Figure 11, as a representative example, to better visualize the morphological aspects of osteocytes observed in all groups at 60 days. Two reversal lines (white arrows) separate the trabecular core (primary bone) from the peripheral part (secondary bone). Note the different morphology of osteocytes as reported in Figure 11. OCL, osteoclast.

occurrence of bone remodeling (Figures 11 and 12), a process that normally allows bone maturation by bone turnover. As it is well known in the literature,[52–56] the process of bone remodeling renews the bone structure for life, thus allowing bone structure/mass adaptation to the actual skeletal requirements: first, the osteoclasts resorb microscopic portions of pre-existing primary bone (mostly woven bone); then, along the erosion cavities, secondary bone (mostly lamellar bone) is deposited by osteoblasts.[52] Thus, the secondary bone is always outlined by a reversal line that represents (i) the point where cellular activity was reversed, and (ii) the demonstration that the bone at 60 days is more mature with respect to the previously secreted primary bone at 30 days, notwithstanding the total amount of bone is almost the same.

A further interesting point, that explains the different histologic fields observed in 30 and 60 days, is related to the existence of two types of osteogenesis, which imply different conditions regarding osteocyte morphology and presence/absence of osteoblasts/osteoclasts. In the last two decades, several authors have highlighted that during intramembranous ossification and bone repair, the well-known dynamic osteogenesis (DO), performed by typical mono-stratified laminae of movable osteoblasts, moving towards the vessels during preosseus matrix secretion, is preceded by static osteogenesis (SO) in which cords of stationary osteoblasts transform into osteocytes in the same place where they differentiated.[42,57–61] SO is devoted to the building of the primary bone of trabecular's core, characterized by woven bone and numerous big globous osteocytes. It is essential for the subsequent DO, performed by typical movable osteoblast laminae present on the trabecular surfaces, thus allowing first the thickening of the primitive trabeculae, and later the bone remodeling with secondary bone formation (after the resorption phase of primary bone by osteoclasts). DO typically leads to the deposition of trabeculae formed mainly by lamellar bone and containing few ovoidal/ellipsoidal osteocytes. Therefore, the low cellularity and more regular collagen texture of secondary bone (i.e., lamellar bone) makes bone more resistant from the mechanical viewpoint with respect to the primary one.[62–66] In this study, the histological findings at 30 days (Figure 10) reflect what happens during the initial stages of bone formation and repair where SO is predominant; in fact, most osteocyte lacunae inside the bone trabeculae are filled by large and roundish osteocytes. At the same time, bone surfaces are mainly covered by movable osteoblastic laminae, involved in the subsequent stages of bone deposition by DO. After 60 days, the histological findings indicate that primary bone trabeculae (previously deposited by SO) have been remodeled: in fact, reversal lines separate the trabecular core of primary bone (Figures 11 and 12), containing roundish osteocytes, from the trabecular peripheral parts (secondary bone) containing ovoidal/ellipsoidal osteocytes, derived from typical laminae of movable osteoblasts. Moreover, also the presence of osteoclasts, numerous close to some bone trabecular surfaces as well as to BG granules, confirms that in our model the bone remodeling is in progress. This process could also explain the significantly lower values of the affinity index, which expresses the BG granules/bone interface, measured at 60 days with respect to 30 days: it is possible that the reshaping of bone trabeculae (depending on bone remodeling) might be responsible for decreasing the contact with the BG granules.

It is also important to point out that this study should be considered preliminary, and that further tests would be necessary. In fact, more samples would be needed, and longer times should be investigated (beyond 60 days) to have a complete long-term study. However, it is worth noting that, for animal studies, the European Commission has adopted the principles already exposed in 1959 when "the three Rs" have been established as the fundamental pillars of animal experimentation. In particular, "Reduction" states that the number of animals involved in studies must be the lowest necessary to achieve scientific evidence.[67,68] So, the small number of animals employed in this study is coherent with the "Reduction" principle and goes in that direction.

Long-term results suggest that resorption of novel BG granules appears to be slower than 45S5 ones; therefore, to better understand the behavior of new BGs, longer experimental times (90 and 120 days after surgery) should be investigated.[69–71] It is important to emphasize that, since BGMS10 and Bio_MS have been recently developed, no data on their dissolution times are available in the literature. Anyways, even if preliminary, this study can be considered as an important indication of the promising in vivo behavior of the novel BGMS10 and Bio_MS. Future work should also include the in vivo investigation of sintered products from these two compositions, such as scaffolds or coatings; in this latter case, residual stresses due to the mismatch of coefficients of thermal expansion between the glass and the substrate should be analyzed.[72,73]

5 | CONCLUSIONS

In the present work, two novel bioactive glasses, namely BGMS10 and Bio_MS, were implanted in rabbits to test their potential regenerative abilities in bone tissue. Whilst after 30 days such BGs have similar performance to 45S5, after 60 days their behavior was quite different. In fact, 45S5 granules were mainly surrounded by wide and scattered bone trabeculae, separated by large amounts of soft tissue; on the contrary, even if the amount of bone was similar, in BGMS10 and Bio_MS the trabeculae were thin and uniformly distributed around the BG granules. Altogether, the novel BG granules have shown to have a good biocompatibility and osteoconductivity. Although these results are preliminary and further investigations will be necessary, the situation observed in BGMS10 and Bio_MS may be considered as more advantageous: indeed, the two novel BG granules allowed for the neo-formation of uniformly distributed bony trabeculae, compared to the less uniform coarse trabeculae, separated by large areas of soft tissue, in 45S5 granules.

These findings suggest that BGMS10 and Bio_MS are promising candidate materials for tissue regeneration, for example, for the realization of products such as coatings and scaffolds for the orthopedic and dental fields.

ACKNOWLEDGMENTS

The authors thank Dr. Marta Benincasa for her technical assistance. Valeria Cannillo and Devis Bellucci acknowledge Progetto FAR 2021 "3D MED" (Dipartimento di Ingegneria "Enzo Ferrari", Università degli Studi di Modena e Reggio Emilia, Italy). The authors declare the following: the bioactive glass Bio_MS (in granules) was patented (Italian patent). Open Access Funding provided by Universita degli Studi di Modena e Reggio Emilia within the CRUI-CARE Agreement.

DATA AVAILABILITY STATEMENT

The data that support the findings of this study are available from the corresponding authors upon reasonable request.

REFERENCES

1. Buser Z, Brodke DS, Youssef JA, et al. Synthetic bone graft versus autograft or allograft for spinal fusion: a systematic review. *J Neurosurg Spine*. 2016;25:509-516.
2. Campana V, Milano G, Pagano E, et al. Bone substitutes in orthopaedic surgery: from basic science to clinical practice. *J Mater Sci Mater Med*. 2014;25:2445-2461.
3. Dec P, Modrzejewski A, Pawlik A. Existing and novel biomaterials for bone tissue engineering. *Int J Mol Sci*. 2023;24:529.
4. Hench LL. The story of bioglass®. *J Mater Sci Mater Med*. 2006;17:967-978.
5. Jones JR. Reprint of: review of bioactive glass: from hench to hybrids. *Acta Biomater*. 2015;23:S53-S82.
6. Miguez-Pacheco V, Hench LL, Boccaccini AR. Bioactive glasses beyond bone and teeth: emerging applications in contact with soft tissues. *Acta Biomater*. 2015;13:1-15.
7. Baheiraei N, Eyni H, Bakhshi B, Najafloo R, Rabiee N. Effects of strontium ions with potential antibacterial activity on in vivo bone regeneration. *Sci Rep*. 2021;11:8745.
8. Naseri S, Lepry WC, Nazhat SN. Bioactive glasses in wound healing: hope or hype? *J Mater Chem B*. 2017;5:6167-6174.
9. Kargozar S, Mozafari M, Hamzehlou S, Baino F. Using bioactive glasses in the management of burns. *Front Bioeng Biotechnol*. 2019;7:62.
10. Lefebvre L, Chevalier J, Gremillard L, et al. Structural transformations of bioactive glass 45S5 with thermal treatments. *Acta Mater*. 2007;55:3305-3313.
11. Boccaccini AR, Chen Q, Lefebvre L, Gremillard L, Chevalier J. Sintering, crystallization and biodegradation behaviour of bioglass®-derived glass–ceramics. *Faraday Discuss*. 2007;136:27-44.
12. Bretcanu O, Chatzistavrou X, Paraskevopoulos K, Conradt R, Thompson I, Boccaccini AR. Sintering and crystallization of 45S5 bioglass® powder. *J Eur Ceram Soc*. 2009;29:3299-3306.
13. Gupta S, Majumdar S, Krishnamurthy S. Bioactive glass: a multifunctional delivery system. *J Control Release*. 2021;335:481-497.
14. Galusková D, Kaňková H, Švančárková A, Galusek D. Early-stage dissolution kinetics of silicate-based bioactive glass under dynamic conditions: critical evaluation. *Materials*. 2021;14(12):3384.
15. Blaeß C, Müller R, Poologasundarampillai G, Brauer DS. Sintering and concomitant crystallization of bioactive glasses. *Int J Appl Glass Sci*. 2019;10(4):449-462.
16. Pedone A, Cannillo V, Menziani MC. Toward the understanding of crystallization, mechanical properties and reactivity of multicomponent bioactive glasses. *Acta Mater*. 2021;213:116977.
17. Mehrabi T, Mesgar AS, Mohammadi Z. Bioactive glasses: a promising therapeutic ion release strategy for enhancing wound healing. *ACS Biomater Sci Eng*. 2020;6(10):5399-5430.
18. Zhu H, Zheng K, Boccaccini AR. Multi-functional silica-based mesoporous materials for simultaneous delivery of biologically active ions and therapeutic biomolecules. *Acta Biomater*. 2021;129:1-17.
19. Vallet-Regi M, Salinas AJ. Mesoporous bioactive glasses for regenerative medicine. *Mater Today Biol*. 2021;11:100121.
20. Drago L, Toscano M, Bottagisio M. Recent evidence on bioactive glass antimicrobial and antibiofilm activity: a mini-review. *Materials*. 2018;11(2):326.
21. Diba M, Tapia F, Boccaccini AR. Magnesium-containing bioactive glasses for biomedical applications. *Int J Appl Glass Sci*. 2012;3:221-253.
22. Gentleman E, Fredholm YC, Jell G, et al. The effects of strontium-substituted bioactive glasses on osteoblasts and osteoclasts in vitro. *Biomaterials*. 2010;31:3949-3956.
23. Hoppe A, Güldal NS, Boccaccini AR. A review of the biological response to ionic dissolution products from bioactive glasses and glass-ceramics. *Biomaterials*. 2011;32:2757-2774.
24. Bellucci D, Cannillo V. A novel bioactive glass containing strontium and magnesium with ultra-high crystallization temperature. *Mater Lett*. 2018;213:67-70.
25. Bellucci D, Veronesi E, Strusi V, et al. Human mesenchymal stem cell combined with a new strontium-enriched bioactive glass: an ex-vivo model for bone regeneration. *Materials*. 2019;12:3633.
26. Bellucci D, Veronesi E, Dominici M, Cannillo V. A new bioactive glass with extremely high crystallization temperature and outstanding biological performance. *Mater Sci Eng C*. 2020;110:110699.
27. International Organization for Standardization. *Biological Evaluation of Medical Devices – Part 5: Tests for in Vitro Cytotoxicity; ISO 10993-5*. ISO; 2009.
28. Kato Y, Windle JJ, Koop BA, Mundy GR, Bonewald LF. Establishment of an osteocyte-like cell kine, MLO-Y4. *J Bone Miner Res*. 2010;12:2014-2023.
29. Karadjian M, Essers C, Tsitlakidis S, et al. Biological properties of calcium phosphate bioactive glass composite bone substitutes: current experimental evidence. *Int J Mol Sci*. 2019;20:305.
30. Bellucci D, Salvatori R, Anesi A, Chiarini L, Cannillo V. SBF assays, direct and indirect cell culture tests to evaluate the biological performance of bioglasses and bioglass-based composites: three paradigmatic cases. *Mater Sci Eng C*. 2019;96:757-764.
31. International Organization for Standardization. *Biological Evaluation of Medical Devices – Part 12: Sample Preparation and Reference Materials; ISO 10993-12*. ISO; 2012.

32. Jurtshuk P. Bacterial metabolism. In: Baron S, ed. *Medical Microbiology*. University of Texas Medical Branch; 1996.
33. Liu X, Rodeheaver DP, White JC, et al. A comparison of in vitro cytotoxicity assays in medical device regulatory studies. *Regul Toxicol Pharmacol*. 2018;97:24-32.
34. Liebsch M, Spielmann H. BALB/c 3T3 cytotoxicity test. In: O'Hare S, Atterwill CK, eds. *Methods in Molecular Biology*. Humana Press; 1995.
35. Czerwińska-Główka D, Krukiewicz K. Guidelines for a morphometric analysis of prokaryotic and eukaryotic cells by scanning electron microscopy. *Cell*. 2021;10:3304.
36. Repetto G, del Peso A, Zurita JL. Neutral red uptake assay for the estimation of cell viability/cytotoxicity. *Nat Protoc*. 2008;3:1125-1131.
37. Wancket LM. Animal models for evaluation of bone implants and devices. *Vet Pathol*. 2015;52:842-850.
38. Pearce AI, Richards RG, Milz S, Schneider E, Pearce SG. Animal models for implant biomaterial research in bone: a review. *Eur Cell Mater*. 2007;13:1-10.
39. Schafrum Macedo A, Cezaretti Feitosa C, Yoiti Kitamura Kawamoto F, et al. Animal modeling in bone research—should we follow the white rabbit? *Anim Model Exp Med*. 2019;2:162-168.
40. Stacchi C, Vercellotti T, Torelli L, Furlan F, Di Lenarda R. Changes in implant stability using different site preparation techniques: twist drills versus piezosurgery. A single-blinded, randomized, controlled clinical trial. *Clin Implant Dent Relat Res*. 2013;15:188-197.
41. Anesi A, Di Bartolomeo M, Pellacani A, et al. Bone healing evaluation following different osteotomic techniques in animal models: a suitable method for clinical insights. *Appl Sci*. 2020;10:7165.
42. Anesi A, Ferretti M, Cavani F, et al. Structural and ultra-structural analyses of bone regeneration in rabbit cranial osteotomy: Piezosurgery versus traditional osteotomes. *J Craniomaxillofac Surg*. 2018;46:107-118.
43. Borenfreund E, Puerner JA. A simple quantitative procedure using monolayer culture for toxicity assays. *J Tissue Cult Methods*. 1984;9:7-9.
44. Berridge MV, Herst PM, Tan AS. Tetrazolium dyes as tools in cell biology: new in-sights into their cellular reduction. *Biotechnol Annu Rev*. 2005;11:127-152.
45. Wang H, Cheng H, Wang F, Wei D, Wang X. An improved 3-(4,5-dimethylthiazol-2-yl)-2,5-diphenyl tetrazolium bromide (MTT) reduction assay for evaluating the viability of *Escherichia coli* cells. *J Microbiol Methods*. 2010;82:330-333.
46. Goodwin CJ, Holt SJ, Downes S, Marshall NJ. Microculture tetrazolium assays: a comparison between two new tetrazolium salts, XTT and MTS. *J Immunol Methods*. 1995;179:95-103.
47. Hench LL. Bioceramics: from concepts to clinic. *J Am Ceram Soc*. 1991;74:1487-1510.
48. Hench LL. Bioceramics. *J Am Ceram Soc*. 1998;81:1705-1728.
49. Abiraman S, Varma HK, Kumari TV, Umashankar PR, John A. Preliminary in vitro and in vivo characterizations of a sol-gel derived bioactive glass-ceramic system. *Bull Mater Sci*. 2002;25:419-429.
50. Davies JE. The use of cell and tissue culture to investigate bone cell reactions to bioactive materials. In: Yamamuro T, Hench LL, Wilson J, eds. *Handbook of Bioactive Ceramics*. CRC Press; 1990.
51. Romanos GE. Biomolecular cell-signaling mechanisms and dental implants: a review on the regulatory molecular biologic patterns under functional and immediate loading. *Int J Oral Maxillofac Implants*. 2016;31(4):939-951.
52. Palumbo C, Ferretti M. The osteocyte: from "prisoner" to "orchestrator". *J Funct Morphol Kinesiol*. 2021;6:28.
53. Hadjidakis DJ, Androulakis II. Bone remodeling. *Ann N Y Acad Sci*. 2006;1092:385-396.
54. Raggatt LJ, Partridge NC. Cellular and molecular mechanisms of bone remodeling. *J Biol Chem*. 2010;285:25103-25108.
55. Delaisse JM. The reversal phase of the bone-remodeling cycle: cellular prerequisites for coupling resorption and formation. *Bonekey Rep*. 2014;3:561.
56. Kenkre JS, Bassett JHD. The bone remodelling cycle. *Ann Clin Biochem*. 2018;55:308-327.
57. Ferretti M, Palumbo C. Static osteogenesis versus dynamic osteogenesis: a comparison between two different types of bone formation. *Appl Sci*. 2021;11:2025.
58. Traini T. The development of the alveolar bone by static osteogenesis: microanatomy and clinical implications. *J Oral Surg*. 2013;4:29-37.
59. Stein K, Prondvai E. Rethinking the nature of fibrolamellar bone: an integrative biological revision of sauropod plexiform bone formation. *Biol Rev*. 2014;89:24-47.
60. Prondvai E, Stein KHW, De Ricqlès A, Cubo J. Development-based revision of bone tissue classification: the importance of semantics for science. *Biol J Linn Soc Lond*. 2014;112:799-816.
61. Cubo J, Hui M, Clarac F, Quilhac A. Static osteogenesis does not precede dynamic osteogenesis in periosteal ossification of Pleurodeles (Caudata, Amphibia) and Pogona (Squamata, Lepidosauria). *J Morphol*. 2017;278:621-628.
62. Boyde A, Riggs CM. The quantitative study of the orientation of collagen in compact bone slices. *Bone*. 1990;11:35-39.
63. Marotti G. The structure of bone tissues and the cellular control of their deposition. *Ital J Anat Embryol*. 1996;101:25-79.
64. Ascenzi MG, Lomovtsev A. Collagen orientation patterns in human secondary osteons, quantified in radial direction by confocal microscopy. *J Struct Biol*. 2006;153:14-30.
65. Ascenzi MG, Gill J, Lomovtsev A. Orientation of collagen at the osteocyte lacunae in human secondary osteons. *J Biomech*. 2008;41:3426-3435.
66. Marotti G, Ferretti M, Palumbo C. The problem of bone lamellation: an attempt to explain different proposed models. *J Morphol*. 2013;274:543-550.
67. Russell WMS, Burch RL. *The Principles of Human Experimental Technique*. Methuen, UFAW; 1959. Accessed April 10, 2020. http://117.239.25.194:7000/jspui/bitstream/123456789/1342/1/PRILIMINERY%20%20AND%20%20CONTENTS.pdf
68. Annex to the Communication from the Commission on the European Citizen's Initiative. *Stop Vivisection*. European Commission; 2015. Accessed April 10, 2020. https://ec.europa.eu/environment/chemicals/lab_animals/pdf/vivisection/en.pdf
69. Zhang L, Ke H, Lin L, et al. Systematic evaluation of the osteogenic capacity of low-melting bioactive glass-reinforced 45S5 bioglass porous scaffolds in rabbit femoral defects. *Biomed Mater*. 2017;12:035010.
70. Khan PK, Mahato A, Kundu B, et al. Influence of single and binary doping of strontium and lithium on in vivo biological properties of bioactive glass scaffolds. *Sci Rep*. 2016;6:32964.
71. El-Rashidya A, Roether J, Harhaus L, Kneser U, Boccaccini AR. Regenerating bone with bioactive glass scaffolds: a review of in vivo studies in bone defect models. *Acta Biomater*. 2017;62:1-28.
72. Cannillo V, Leonelli C, Boccaccini AR. Numerical models for thermal residual stresses in Al_2O_3 platelets/borosilicate glass matrix composites. *Mater Sci Eng A*. 2002;323:246-250.
73. Cannillo V, Montorsi M, Siligardi C, et al. Microscale computational simulation and experimental measurement of thermal residual stresses in glass-alumina functionally graded materials. *J Eur Ceram Soc*. 2006;26:1411-1419.

How to cite this article: Anesi A, Ferretti M, Salvatori R, et al. In-vivo evaluations of bone regenerative potential of two novel bioactive glasses. *J Biomed Mater Res*. 2023;1-15. doi:10.1002/jbm.a.37526